Available online at www.sciencedirect.com
SCIENCE DIRECT®
International Journal of Mass Spectrometry 232 (2004) 67–77
International Journal of Mass Spectrometry
www.elsevier.com/locate/ijms

Tandem mass spectrometry study of protonated methanol–water aggregates

Phillip Jackson*

Research School of Chemistry, Science Road, Australian National University, Canberra, ACT 0200, Australia

Received 8 July 2003; accepted 21 November 2003

Abstract

Protonated nanodroplets containing methanol (M) and water (W) solvent monomers (up to $M_{23}W_{41}H^+$) have been generated using electrospray ionisation (ESI) in conjunction with both high-solvent and low-drying gas-flow rates in a triple quadrupole mass spectrometer. Under the conditions employed, pure methanol clusters (M_mH^+) dominate the low-mass region of the spectrum ($m < 7$). When the number of methanol monomers exceeds seven, a rapid increase in the addition of water to the clusters was observed, and a 1:1 mole ratio is achieved for $m = 11$ ($M_{11}W_{11}H^+$). The variation of the summed ion current with the total number of monomers $m + n =$ constant, where m and n represent the number of methanol and water molecules, respectively, was found to peak after repeated additions of five or six units, implying rings could be a structural feature of these mixed clusters [Garvey and coworkers, J. Am. Chem. Soc. 114 (1992) 3684].

The low-energy collision-induced dissociation (CID) chemistry of selected nanodroplets up to $m/z = 600$ has also been investigated, and the gentle nature of this approach has enabled some characterisation of the outermost solvation shells. Unexpected ion–molecule chemistry involving substitution of outer shell methanol molecules by water (present as a small component of the CID gas) suggests that even in large $M_mW_nH^+$ clusters some methanol molecules occupy positions at the droplet periphery. CID evidence was also found for competitive solvation of the proton, although dehydration of mixed clusters to yield methanol cores is by far the most thermodynamically favourable process.

Keywords: Water–methanol clusters; Collision-induced dissociation; Triple quadrupole

1. Introduction

It has been amply demonstrated that protonated molecular clusters comprising solvent monomers (e.g., H_2O, CH_3OH, C_2H_5OH, CH_3CN) can be generated using conventional ionisation approaches, such as fast atom bombardment (FAB) [1–4], liquid secondary ion mass spectrometry (LSIMS) [5], and APCI [6,7], or by dilution of a suitable vapour mixture in an inert gas flow with subsequent gas pulsing/sampling and ionisation [8–22]. Alternately, protonated monomers in the presence of solvent vapour can act as nucleation centres for the synthesis of molecular clusters, such as neat and mixed dimers, trimers, etc. [23,24].

Past studies of protonated methanol and methanol–water clusters have been concerned with (i) the development of models to describe ionisation mechanisms [1–3,5] and dissociation mechanisms [15,16,25], (ii) the derivation of thermochemical values, such as gas phase basicities [9,11,12,18], and (iii) understanding the microstructure of both pure solutions and binary mixtures [14,19–21,26]. Extensive ion–molecule equilibria studies at various temperatures have generated values for the heats and free energies of formation of pure and mixed clusters [9,11,12,18,23,26], as well as information about the extent of solvation shells. Relative cluster abundances in broad-scanned mass spectra have also been used to identify solvent shell closures, as inferred from 'magic numbers' or high peak counts [9,19]. For $(H_2O)_nH^+$ and $(CH_3OH)_mH^+$, the first solvation shells are closed when $n = 4$ and $m = 3$, respectively [9]. $(H_2O)_{21}H^+$ is another cluster of high stability [19,27], and a dodecahedral structure with a central H_3O^+ core has been proposed [27].

From studies of water-doped methanol clusters (mixed dimer through to $(CH_3OH)_m{\cdot}H_2O{\cdot}H^+$, $m \leq 25$ [7,10,28]),

* Present address: Isotope and Organic Geochemistry Laboratory, Geoscience Australia, Cnr Hindmarsh Drive and Jerrabomberra Avenue, Symonston, ACT 2609, Australia. Tel.: +61-2-6249-9005; fax: +61-2-6249-9961.
E-mail address: phillip.jackson@ga.gov.au (P. Jackson).

1387-3806/$ – see front matter © 2003 Elsevier B.V. All rights reserved.
doi:10.1016/j.ijms.2003.11.007

Table 1
Thermodynamic and electric properties of methanol and water

Property	CH_3OH	H_2O
ΔH_f° (kJ/mol)	−201[a]	−241.826 ± 0.040[b]
PA (kJ/mol)[b]	754.3	691
ΔG_B (kJ/mol)[b]	724.5	660
μ (D)[c]	1.70	1.85(4)
α' (Å^3)[c]	3.23	1.48

[a] From Ref. [35].
[b] From Ref. [36].
[c] From Ref. [37].

the early consensus was that, up to a certain size, the proton in these species is likely to be methanol-centred, i.e., $CH_3OH_2^+$, and that water molecule(s) in small mixed methanol–water clusters (<9 molecules) were remote from the charge centre. For some particular methanol cluster size, water addition to the outermost solvation shell begins to compete energetically with further methanol addition, in accordance with relative dipole moments and polarisabilities (see Table 1). According to Stace and Shukla [10], this occurs when the number of monomers ∼9. Garvey and co-workers [17] were early advocates of small methanol–water clusters with H_3O^+ centres, and recently published results have verified their existence [29]. For $n + m \leq 6$, Kebarle and co-workers [8] have argued there is no distinct preference for either water- or methanol-centred protons in small, mixed $M_mW_nH^+$ clusters.

Very recent vibrational predissociation-MS experiments performed to interrogate the mixed cluster $(H_2O)(CH_3OH)_4H^+$ [29], have confirmed the presence of at least two structural isomers, and as mentioned above, one that is water-centred. Density functional theory calculations performed by the authors to support their spectral assignments, resulted in the location of *seven isomers within 1.3 kcal of the global minimum*. It is clear that for most, if not all, of the clusters investigated in this and previous articles, an isomer average has been sampled experimentally. While this may act as a deterrent to further investigations, a number of vexing questions concerning mixed methanol–water aggregates remain unanswered, including (i) the cluster size at which addition of water competes with methanol addition, (ii) how many monomer units are required to close outer solvation shells, which is implicitly related to the extent of branching, and (iii) can collision-induced dissociation (CID) be used to characterise clusters containing both water- and methanol-centred protons?

Low-energy CID results for mixed clusters $(H_2O)_n(CH_3OH)_mH^+$, generated using electrospray ionisation (ESI), are presented in the following sections. Previously, Karpas et al. [7] have dissociated protonated methanol clusters containing a single water impurity (up to $m = 9$) using a triple quadrupole mass spectrometer. For all clusters dissociated, water retention was disfavoured relative to water expulsion. The following report focuses on the dissociation behaviour of clusters with one proton and one or more water molecules in the mass range 300–600 Da. Experiments were performed under single- and multiple-collision conditions. The collision energies used in this study are relatively low, as it is desirable to desolvate the clusters, monomer by monomer, whilst avoiding covalent disruption to individual solvent units. This energy regime allows for the investigation of the most stable entities on the adiabatic (single electronic) desolvation surface, and under multiple-collision conditions, all but a few of the monomer units can be evaporated from the original protonated cluster. Unlike previous electron ionisation (EI), FAB and LSIMS studies, which rely on rather extreme (non-equilibrium) conditions to generate protonated ions, the clusters formed in this study were originally subunits of much larger droplets with a large excess of charge. Through successive evaporative and charge-induced dissociations, the original droplets were shrunk to nanosize monocharged aggregates. Due to the efficient conversion of internal energy to fragment (neutral plus ion) kinetic energy during source dissociations, it can be assumed that the mass-selected clusters have internal energies close to the source temperature (353 K).

This work was performed with the notion of developing a better understanding of the outer solvation shell structure(s) and the potential for competitive proton solvation in small nanoscale droplets.

2. Experimental

All experiments were performed on a VG-Fisons Quattro II triple-quadrupole mass spectrometer equipped with a pneumatic ESI source and a Hewlett-Packard 1090 high performance liquid chromatograph (HPLC) solvent delivery system. For the optimal generation of the methanol–water clusters investigated, a solvent flow rate of >0.09 ml/min was necessary with a composition of 85–98% CH_3OH. Filtered deionised water was used throughout, together with HPLC-grade methanol (Merck, >99.99% purity). The nebulising and drying gas-flow rates (dry N_2 from cryogenic boiloff, 50 and 75–500 l/h, respectively) were also adjusted for optimal yields of specific clusters. As the instrument is routinely used to study natural products and synthetic chemical work-ups, the stainless steel electrospray capillary was flushed with 50:50 aqueous methanol for 12 h prior to these studies. To further reduce the abundance of ammonium-centred solvent clusters, the fused silica capillary, which carries the solvent flow to the ESI probe, was replaced prior to experiments.

For a discussion of the principles and theory of ESI, see Ref. [30]. The needle voltage required to induce charged droplet formation was varied between 3.2 and 4.3 kV. The droplets emitted from the capillary tip enter into a desolvation chamber which consists of a stainless steel cylinder (resistively heated to 80 °C) electrically isolated from the ESI probe by plastic mountings. All experiments were performed at this source temperature. The desolvation gas flow

into this chamber maintains the pressure at, or close to, 1 bar. The ions exit this region through off-axis chicanes in the end-plate of the jacket ('pepper pot', grounded to the instrument chassis) and enter into a second desolvation region, also at, or near 1 bar. After traversing approximately 10 mm, the ions exit through a 100 μm aperture in the cone plate, and travel 3 cm to the first of several focussing elements. The dc voltages applied to these elements were low in magnitude, always <5 V. An rf-hexapole/ion guide focussed the ions onto the first of two mass-resolving quadrupoles. The voltage on the cone plate was varied in the range −20 to −100 V in order to maximise cluster yields. Quadrupole 1 was either scanned (for broad range mass analysis) or parked at a predetermined *m*/*z* value for MS^2 studies (discussed below). The dc/rf ratio was adjusted such that the resolution was at least M/ΔM fwhm 500, and the dc rod offset set to zero to avoid unnecessarily imparting kinetic energy to exiting ions. In the mass-scanning mode, ions were deflected onto a dynode/phosphor/photomultiplier assembly, and the signal amplified and correlated with the scan rate to produce the mass spectrum.

For MS^2 studies, Q1 was 'parked' at the mass-of-interest. Following transmission, mass-selected ions were extracted into a gas cell containing an rf-only hexapole, of length 16 cm. The pressure inside the gas cell (argon, >99.9% purity, CIG gases), after admission of the target gas, was one to two orders of magnitude higher than the background analyser pressure ($<2.5\times10^{-6}$ mbar, uncorrected). The analyser pressure was observed to increase 2×10^{-7} to 3×10^{-7} mbar upon admission of the collision gas indicating the collision cell design is not 'gas tight'; mass-selected ions could well undergo collisions before entering the cell, particularly if KE_{ion} is low. The collision gas was admitted through a needle valve to a pressure of 2.0×10^{-4} mbar (predominantly single-collision conditions, >85% parent beam transmission) or up to 6.0×10^{-4} mbar (multiple collisions for reasonable yields of low-mass daughter ion currents).

The voltages applied to the four focussing lenses preceding the collision cell were measured using the null method with a Fluke digital voltmeter and Fluke 341A dc voltage calibrator. Variation of measured values with changes in various source voltages were less than 0.01%. In order approaching the collision cell from Q1, the measured values for each lens is: lens 5 = −101.31 ± 0.01 V, lens 6 = −2.761 ± 0.005 V, lens 7 = −252.30 ± 0.01 V, lens 8 = −230.685 ± 0.005 V. A dc voltage applied to the metal case of the rf-only gas cell determined the final ion collision energy; this voltage was also measured using the null method. Finally, after traversing the gas cell, the parent ions and any fragments were extracted by voltages applied to lens 9 and a prefilter lens, before entering a second mass-resolving quadrupole, which was scanned over the mass range of interest. The voltages applied to lens 9 and the prefilter are functions of the dc collision cell voltage and the mass-selected parent ion [31]. Undoubtedly, the field resulting from the voltage applied to lens 9 will fringe, to a limited extent, into the collision cell. It is unclear how this voltage affects the overall collision energy; for this report, it is assumed the fringing field has a negligible effect. The collision energies presented are corrected for the centre-of-mass reference frame. Ions transmitted through quadrupole 2 were measured with a dynode/phosphor/photomultiplier detector assembly (as for Q1) and the signals correlated with the scan rate. The mass scale was calibrated for both scanning quadrupoles using an aqueous mixture of caesium and sodium iodide salts which, when electrosprayed, gives rise to clusters of the form $(CsI)_nCs^+$.

All adjustable voltages were set within the Masslynx 3.5 software suite [32]; this software was also used to acquire and process spectra. The software was run on a Compaq-PC running Windows NT, with 12 GB memory and a processor speed of 300 MHz.

3. Results and discussion

3.1. Cluster distribution and magic numbers

Typical cluster spectra obtained by scanning quadrupole 1 (average of 30 scans), are presented in Fig. 1. The cluster distribution observed is the result of incomplete desolvation at high-solvent and low-drying gas-flow rates. Reduction of the solvent flow rate to less than 0.09 ml/min effectively quenches formation of the higher mass mixed aggregates, however the neat protonated methanol clusters (up to M_6H^+, where M = CH_3OH) were persistent even at lower flow rates (0.07 ml/min). Depending on the flow rate, either M_3H^+ or M_4H^+ was the base peak in the spectrum, with formation of the tetramer favoured at higher flow rates. Under optimal conditions for larger droplet formation, peaks up to $m/z \sim 1500$ were observed. Due to the near exponential decrease in cluster abundance with increasing mass, the highest peak which could confidently be assigned was m/z = 1474, $M_{23}W_{41}H^+$. Only a few hundred ion counts were recorded for aggregates above about $m/z = 600$, effectively precluding CID studies. For example, the abundance of $M_{23}W_{41}H^+$ relative to M_3H^+ was measured to be 0.024%. Previously, the FAB of frozen methanol–water samples was used to generate protonated clusters containing up to 30 monomer molecules ($M_{22}W_8H^+$) [5]. The low-mass portion of the positive-ESI spectrum is essentially identical to spectra obtained using this approach, with the exception of radical cluster ions and abundant hydrated clusters containing fewer than seven methanol molecules. Clearly, the FAB covalent bond rupturing, as evidenced through the detection of radical cluster ions ($-H_{1–3}$), confirms this technique is not as 'soft' as ESI, even though there are many similarities in the spectra produced using the two methods. The more energetic nature of FAB/LSIMS also accounts for the reduced extent of the distribution, as the clusters would have a higher effective temperature and be prone to evaporative desolvation.

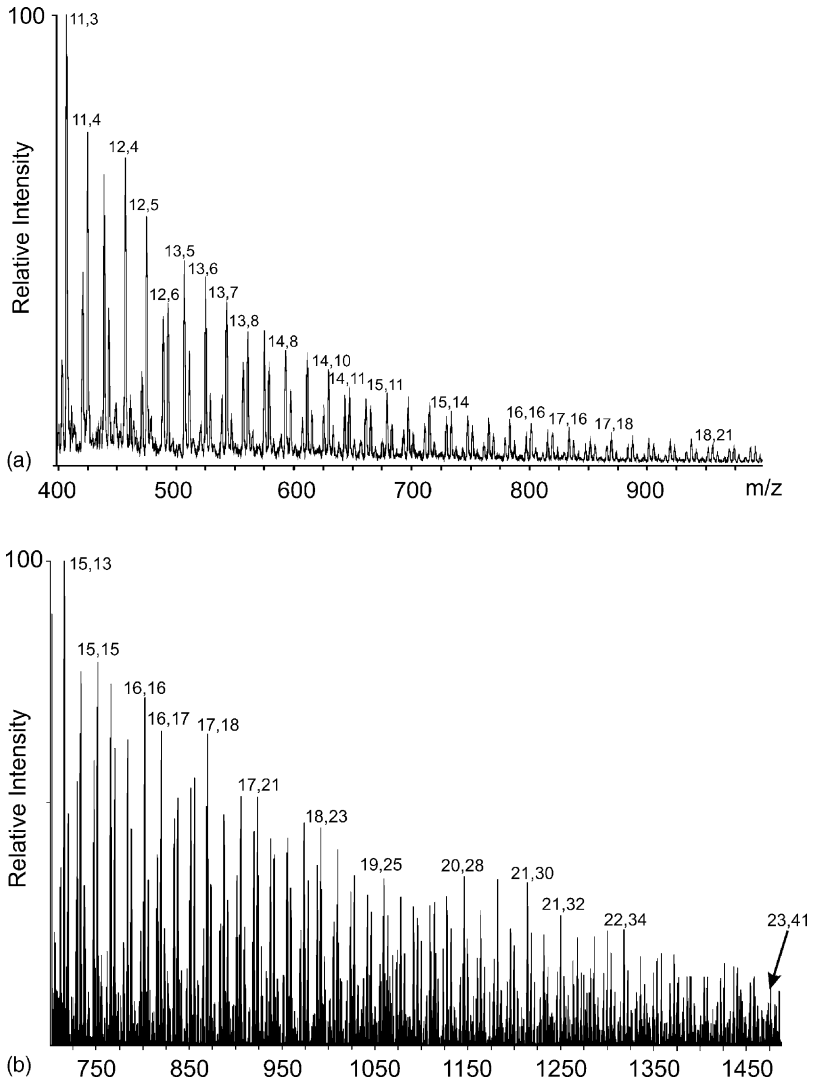

Fig. 1. Cluster distributions obtained for $M_mW_nH^+$ clusters (in the figure at m/z = 679, 15,11 = $(CH_3OH)_{15}(H_2O)_{11}H^+$) using positive-ESI and a high-solvent flow rate with the source temperature fixed at 80 °C. The bottom figure shows the distribution extending up to m/z = 1500.

A plot of the cluster stoichiometries assigned in these experiments is presented in Fig. 2. It can be seen that the smallest cluster to attach a water molecule is $M_8W_1H^+$. The ratio of water to methanol increases dramatically for aggregates containing eight or more methanol molecules, and a cluster with a 1:1 M:W ratio is observed at $n = m =$ 11. Pure water clusters W_nH^+ were not observed under the solvent flow conditions used to generate high yields of the mixed clusters $M_mW_nH^+$.

Without inferring any immediate connection, structural or otherwise, the ESI spectra above m/z = 600 are characterised by groups of three peaks, referred to in the following paragraphs as 'triplets'. Adjacent triplet groupings are separated by either 6 or 10 Da. The three peaks within the triplets are separated by 4 Da, and the peak compositions are detailed in Scheme 1.

There is no correlation between the abundances of neighbouring peaks within these groupings, although there is potentially a compositional relationship between adjacent triplets that could be a consequence of outer shell substitutional chemistry [19], a theme which will be explored further below.

If substitutional chemistry is operative, insights into shell closures can be discerned through a plot of the number of solvent molecules ($n+m$ = constant) versus the log of total abundance (for $n+m$), as presented in Fig. 2 (bottom). As an example, for $n+m$ = 15, the abundances (relative to M_3H^+) of the following peaks were summed: ($M_mW_nH^+$, m, n) = 11,4; 12,3; 13,2.

Near linear decreases in the natural logarithm of cluster abundances are evident in the plot. In addition, breaks from linearity occur with the addition of five to six solvent molecules, e.g., 13 → 18, 21 → 26, 32 → 37, 40 → 45, 48 → 53, 53 → 58 as indicated in the figure, supporting the suggestion of Garvey and co-workers [17] that rings could be a structural feature of mixed methanol–water clusters.

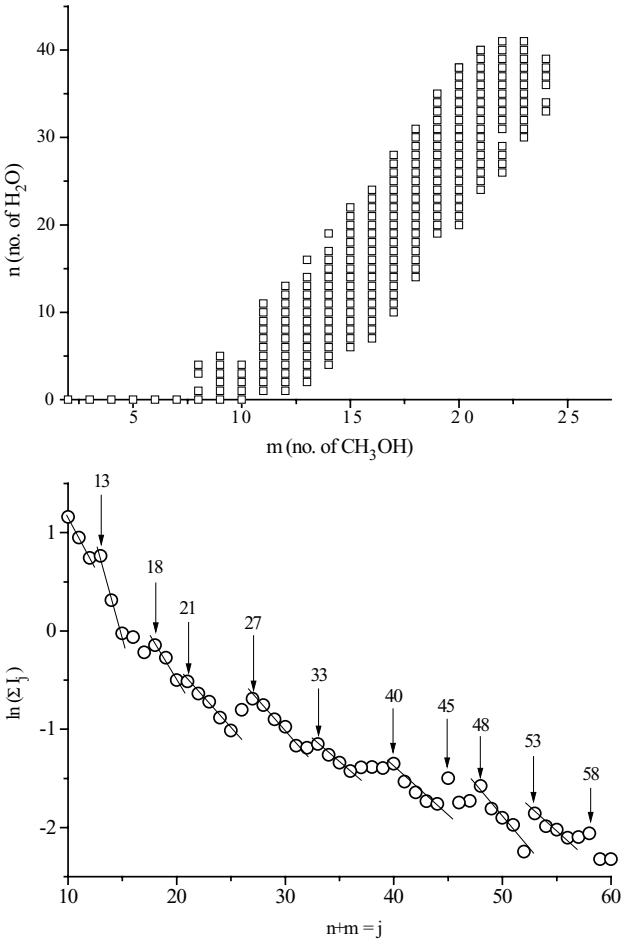

Fig. 2. (Top) Plot of the methanol–water cluster stoichiometries observed in the positive-ESI experiments. (Bottom) Plot of the natural logarithm of the cluster intensity (abundance) sum for $n + m =$ constant, where n and m = number of water and methanol molecules, respectively.

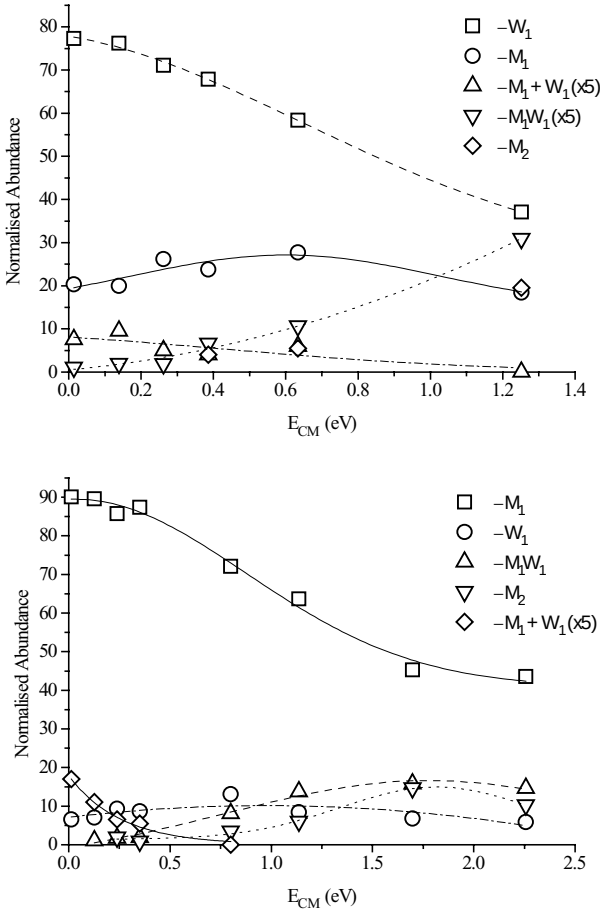

Fig. 3. CID profiles for M_8WH^+ (top) and M_9WH^+ (bottom) obtained under single-collision conditions using argon as a collision gas.

Saykally [33] has presented experimental results for the existence of small, cyclic (neutral) methanol clusters, and Chaudhuri et al. [29] computational evidence for cyclic, protonated mixed clusters, although entropically these are disfavoured relative to extended isomers. It is not clear from the diagram if the addition of five or six monomers is preferred, probably as a result of the ability of several water molecules to occupy a single methanol site. There is also an indication of enhanced stability for $m + n = 21$ [19,27], but it is not as pronounced for the mixed methanol–water system as it is for pure water, as the latter is more ordered.

3.2. Collision-induced dissociation

Firstly, the single CID of selected clusters with sizes approaching the regime where the proton–water attractive potential (according to Eq. (1), see below) becomes greater than the proton–methanol attractive potential, are discussed. A more general discussion of the single and multiple CIDs of larger, more hydrated clusters follows.

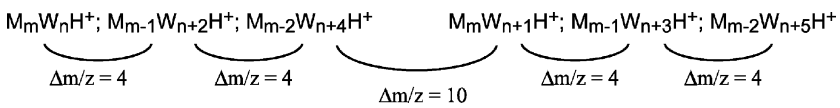

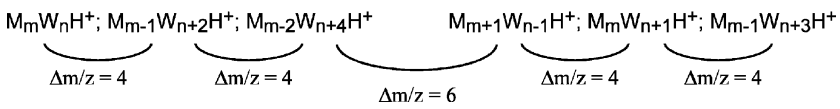

Scheme 1.

3.2.1. $M_8W_1H^+$, $M_9W_1H^+$

The CID profiles for these particular clusters (see Fig. 3), obtained under single-collision conditions, can be compared to those published by Karpas et al. [7]. With reference to Fig. 3, it can be seen that, as the centre-of-mass collision energy (E_{CM}) increases, the abundance of the water loss daughter (the most abundant CID product) from $M_8W_1H^+$ decreases almost linearly. Water loss from this cluster appears to be exothermic even at low-collision energies, and the high abundance of this daughter may also result from metastable processes. Since it is not possible to bake out the analyser region of the Quattro II, and the collision cell itself is not gas tight, metastable transitions are alluded to, but not explicitly assigned.

The daughter corresponding to methanol loss from $M_8W_1H^+$ initially increases in abundance with increasing energy but then plateaus, suggesting a slight barrier for this process. Loss of M_2 and M_1W_1 from $M_8W_1H^+$ become favourable above $E_{CM} = 0.36$ eV. The absolute energies required for the smaller water-doped cluster $M_5W_1H^+$ to evaporate M_2 and M_1W_1 are 24.8 and 23.5 kcal/mol, respectively [11], so the experimental results for the evaporation of two monomer units from $M_8W_1H^+$ (reaction enthalpies of similar or lower magnitude) are in accordance with expected thermochemistry.

Under multiple-collision conditions (<50% transmittance) at $E_{CM} = 0.63$ eV, quite extensive fragmentation of $M_8W_1H^+$ was induced. The smallest fragment detected was $m/z = 63$, or $M_1W_1H^+$. In a similar fashion to Karpas et al. [7], abundance calculations show that only 8% of the fragment ion current retained the water molecule (cf. 20% [7]). Moreover, the abundance of $M_mW_1H^+$ decreased

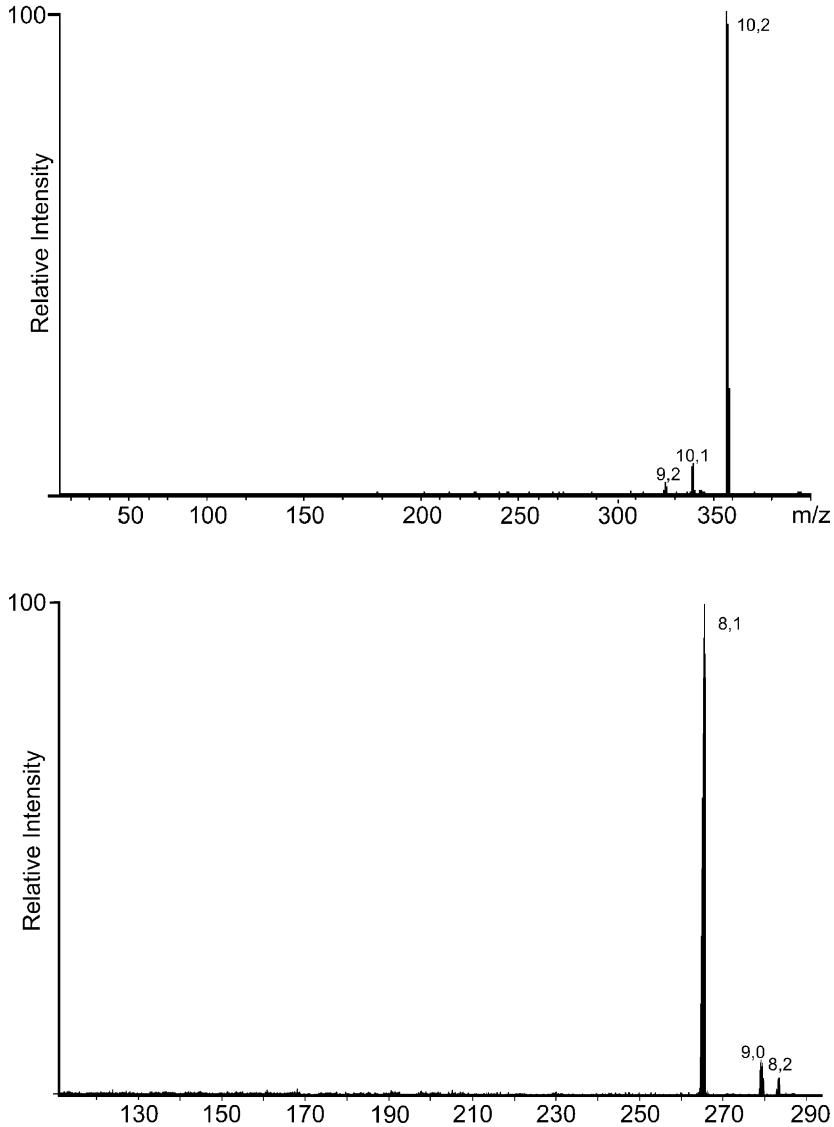

Fig. 4. Single-collision CID spectra for $M_{10}W_2H^+$ (top) at $E_{CM} = 0.011$ eV and M_9WH^+ (bottom) at $E_{CM} = 0.012$ eV. While loss of water is preferred for $M_{10}W_2H^+$, this is clearly not the case for M_9WH^+. The M → W substitution product $M_8W_2H^+$ is evident in the CID spectrum of $M_9W_1H^+$.

sharply for $m < 7$, i.e., $M_7W_1H^+$ contributes over 55% of the total water-retaining fragment ion current.

With reference to Fig. 3 (bottom) and Fig. 4 (top), the results for $M_9W_1H^+$ indicate that methanol loss is favoured for this cluster. As E_{CM} increases from the lowest values, the abundance of the methanol daughter product begins to decrease, suggesting an exothermic reaction and the early onset of other accessible fragmentation channels. In contrast, there is a barrier associated with water loss from this cluster. Above $E_{CM} \sim 0.7$ eV, loss of multiple monomer units becomes significant. Multiple-CID conditions reveal only 15% of daughter ion current retains the water molecule, and of this 15%, more than 55% presents as $M_{7,8}W_1H^+$. Aside from this, the most interesting aspect of the CID chemistry for this cluster is the preferred loss of methanol, rather than water. This concurs with the metastable results of Stace and Shukla [10], and potentially marks the transition to preferential water addition to the outermost solvation shells. Fig. 2 (top) also supports facile hydration at this cluster size. Using the two-term attractive (central) potential [34]:

$$V_{\text{eff}} = \frac{-\alpha q^2}{2r^4} - \frac{\mu_D q}{r^2} \quad (1)$$

where r, radial distance of monomer from the proton, α, monomer polarisability, μ_D, monomer dipole moment and q, electron charge, together with the relevant values from Table 1, the potential due to the proton becomes more attractive for water at a distance of ~5.5 Å. It is quite likely that two of the solvent molecules (the water and a methanol) associated with $M_9W_1H^+$ reside at, or near, this distance from the proton core of the cluster.[1]

The other noteworthy features of Fig. 3 (and subsequent CID profiles) and Fig. 4 (bottom) are the low-energy ion–molecule chemistries involving methanol substitution by water. Water is always present in mass spectrometers, and condenses on cold surfaces when instruments are vented to atmosphere. Instrument baking may alleviate this problem to some extent, but will not completely remove the water. As expected, as E_{CM} increases, the abundance of the ion–molecule reaction product decreases. The maximum yield of the substitution product for either ion does not exceed 0.7% of the total parent ion current. Nonetheless, this result confirms the 'substitutional interaction' characteristic of the methanol–water system proposed by Wakisaka et al. [19]. Substitution can also be used to ascertain the existence of methanol molecules residing on the cluster surface, as will be explained further below

3.2.2. $M_{10}W_1H^+$, $M_{10}W_2H^+$, $M_{11}W_1H^+$

The CID profiles for $M_{10}W_1H^+$ and $M_{10}W_2H^+$ are presented in Fig. 5, and the CID spectrum of $M_{10}W_2H^+$

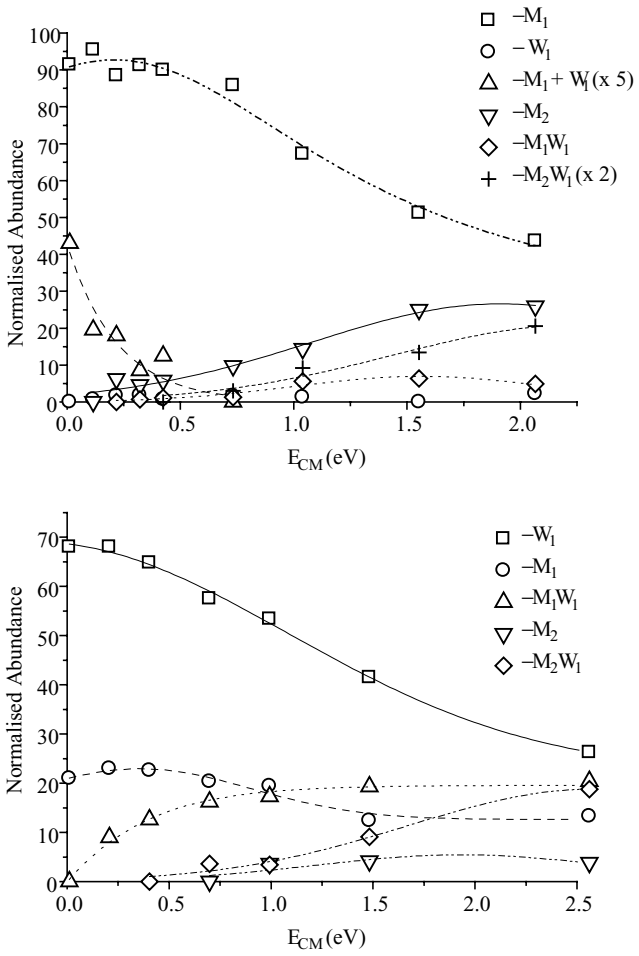

Fig. 5. CID profiles for $M_{10}WH^+$ (top) and $M_{10}W_2H^+$ (bottom).

under single-collision conditions, is presented in Fig. 4. While water loss is disfavoured relative to methanol loss for $M_9W_1H^+$, water loss is not kinetically competitive with methanol loss for $M_{10}W_1H^+$; moreover, loss of two methanol molecules is observed at lower energies than loss of both a methanol plus the water. Together with the relatively high concentration of the M → W substitution product at low E_{CM}, there appears to be two methanol molecules on the cluster periphery, and at least one of these methanol molecules occludes the water molecule. It would seem that the size for which water addition becomes more favourable than methanol addition has been achieved.

Water loss is the dominant fragmentation channel for $M_{10}W_2H^+$, and decreases with increasing E_{CM}. The abundance of the M_1 loss daughter can be seen to slightly increase as E_{CM} increases, but then tails off as loss of multiple monomer units becomes energetically accessible. Fig. 5 indicates methanol loss is slightly endothermic, whereas water loss is less energy demanding. The other noteworthy feature of the CID chemistry of $M_{10}W_2H^+$, is the absence of significant quantities of the substitution product $M_9W_3H^+$, which confirms one or both of the water molecules are at the cluster periphery. The most likely monomer unit ordering,

[1] The application of this equation assumes the charge is localised. Although this is not entirely realistic, many experimental observations, such as the preference for M_mH^+ cores, are readily explained using this equation.

Table 2
Low-energy CID results for proton-bound mixed methanol–water clusters

$M_mW_nH^+$, *m,n*[a]	Range (loss M_1:loss W_1)		M → W maximum (%FIC)	Maximum monomers lost (*T*)		
	Low E_{CM} limit	Minimum (E_{CM}/eV)		$T = m + n$	*m*	*n*
8,1	0.20:0.77	0.18:0.37 (1.25)	1.9	4	3	1
9,1	0.90:0.07	0.72:0.13 (0.80)	3.4	5	4	1
10,1	0.91:0.00	0.44:0.02 (2.07)	8.6	5	4	1
10,2	0.21:0.68	0.13:0.26 (2.56)	≪1	5	3	2
11,1	0.80:0.00	0.43:0.00 (2.47)	20.1	5	4	1
11,2	0.61:0.25	0.25:0.12 (2.37)	14.1	6	4	2
10,3	0.26:0.60	0.17:0.33 (1.42)	17.7	5	3	2
11,3	0.39:0.50	0.17:0.37 (1.32)	6.5	5	3	2
					2	3
11,4	0.19:0.70	0.23:0.49 (0.76)	12.1	6	3	3
12,3	0.45:0.32	0.23:0.17 (1.63)	22.6	7	4	3
11,5	0.22:0.74	0.09:0.25 (2.11)	4.2	6	3	3
12,4	0.43:0.48	0.31:0.30 (1.18)	8.6	6	3	3
13,3	0.60:0.20	0.38:0.26 (1.15)	20.0	4	3	1
12,5	0.39:0.52	0.29:0.18 (1.52)	7.8	6	4	2
					2	4
13,4	0.66:0.26	0.47:0.34 (0.60)	8.7	5	2	3
					3	2
12,6	0.20:0.74	0.12:0.26 (1.91)	6.2	7	3	4
					4	3
13,5	0.58:0.37	0.30:0.47 (0.36)	8.0	6	2	4
13,6	0.44:0.53	0.27:0.31 (1.04)	4.4	6	3	3
14,5[b]	0.57:0.32	0.32:0.29 (1.35)	11.1	3	3	0
					2	1
					1	2
14,6[b]	0.65:0.23	0.36:0.39 (0.66)	5.9	3	1	2
13,7	0.43:0.56	0.33:0.46 (0.68)	3.2	5	2	3
					3	2
12,9	0.10:0.69	0.08:0.27 (1.73)	21.3	6	3	3
13,8	0.26:0.62	0.35:0.44 (0.66)	6.0	6	3	3
14,7	0.35:0.50	0.41:0.30	15.4	6	4	2
14,8	0.30:0.70	0.42:0.40 (0.32)	5.7	5	1	4
					3	2
13,9	0.16:0.80	0.32:0.51 (0.64)	4.7	5	2	3
					1	4

The extent to which CID loss of M vs. W and the substitution reaction M → W varies, are expressed as percentages of the measured fragment ion current (FIC). Parents for which methanol monomer loss is kinetically preferred to water monomer loss, are italicised.
[a] Italicised rows are for ions where methanol loss is preferred.
[b] Results signal limited, low parent ion counts.

according to radial distance from the proton (counting inwards from the periphery of the cluster), is W–M–M–W · · · . It is doubtful that the structure proposed by Garvey and co-workers [17], in which the core of the cluster possesses an $H_5O_2^+$ unit, could yield the observed product distribution, particularly the facile loss of a water monomer.

For $M_{11}W_1H^+$, water loss is always accompanied or preceded by methanol loss up to $E_{CM} \cong 2.5$ eV. The substitution product is relatively abundant, even at higher E_{CM}'s:

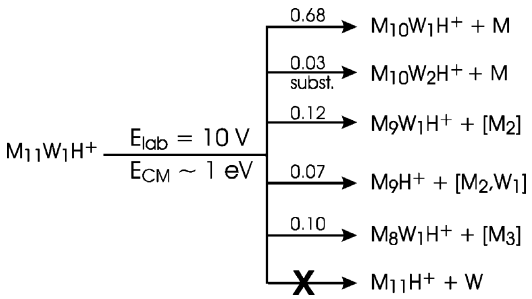

Together the results suggest that the water molecule in this cluster is occluded by at least one methanol monomer.

3.2.3. Other clusters: single-collision regime

The results for other clusters studied are presented in Table 2 and Fig. 6. Quite unexpectedly, there are a number of species containing water, and some with high water contents, for which methanol loss is kinetically preferred to water loss, e.g., $M_9W_1H^+$, $M_{12}W_3H^+$, $M_{13}W_4H^+$, $M_{14}W_5H^+$, $M_{14}W_6H^+$, italicised in Table 2. This suggests that, once the cluster extends beyond the region where the attractive force due to monomer polarisability is dominant, any preference for either water or methanol retention is structure dependent. Although the central potential Eq. (1) suggests water addition is apparently more favourable at a radius that exceeds ∼5.5 Å, methanol molecules can also be found in the outermost solvation shells; however, the outer regions of these clusters are indisputably water-enriched, as confirmed

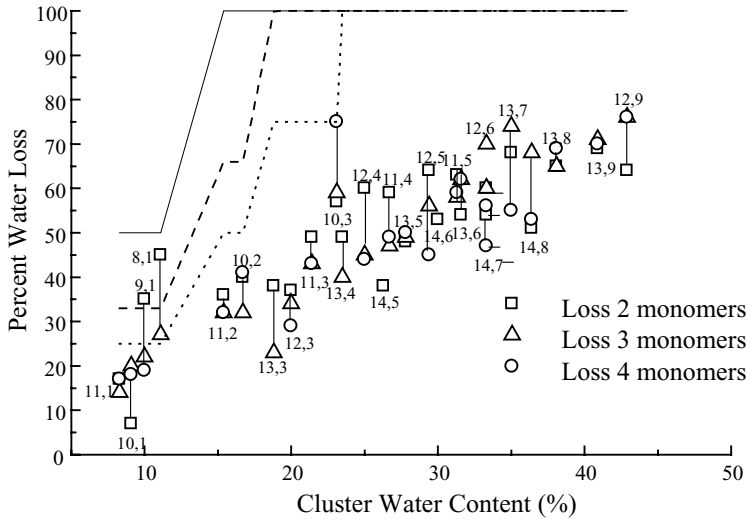

Fig. 6. Plot of the water loss fragment ion current (*y*-ordinate, expressed as a percentage of the total fragment ion current) vs. cluster water content (*x*-abscissa) for the aggregates investigated in CID experiments. The lines towards the top of the figure represent the total allowable water loss for the cluster compositions investigated: solid, loss of two monomers; long dash, loss of three monomers; short dash, loss of four monomers. Short lines connect data points for a given cluster. The plot indicates smaller methanol-enriched clusters dehydrate most efficiently.

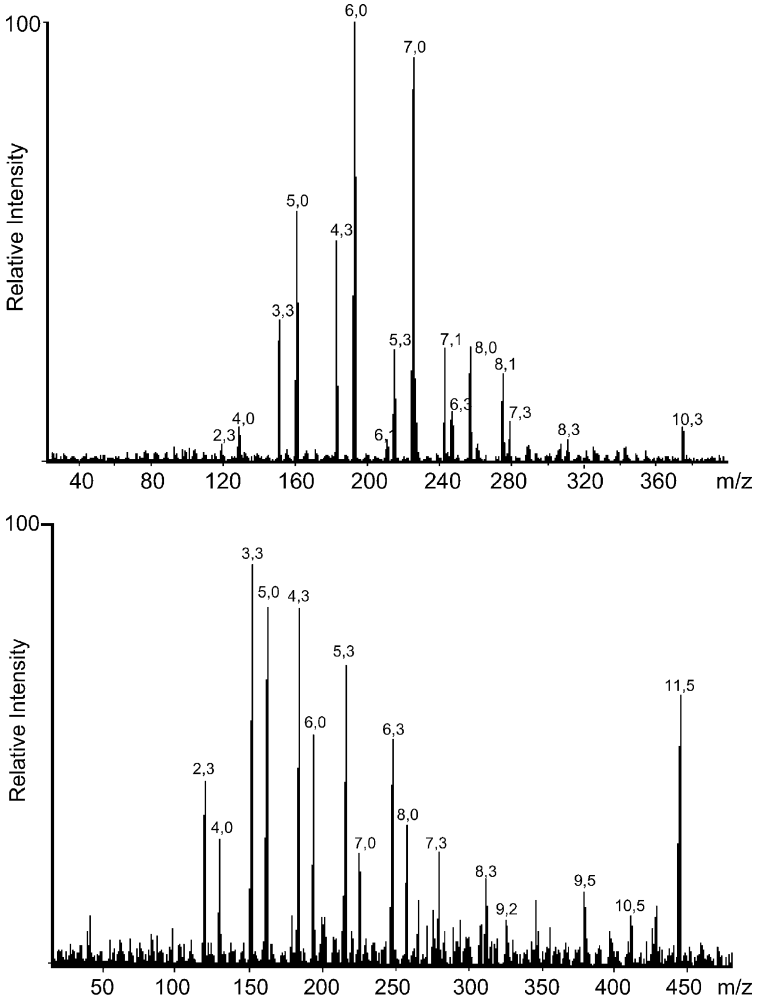

Fig. 7. Multiple-CID spectra for $M_{10}W_3H^+$ (top) and $M_{11}W_5H^+$ (bottom). Note the intense fragment peaks corresponding to $M_mW_3H^+$ in both spectra; the M_mH^+ series was observed to dominate the low-mass region of CID spectra for most other clusters. The absence of significant fragment ion populations of $M_mW_yH^+$, where $y = 1$, 2 or 4, suggests that there is competitive solvation of the proton by water in certain geometric isomers of these stoichiometries.

by the higher water content of the fragment ion current for $M_mW_{n>3}H^+$ (Fig. 6).

With reference to Fig. 6, although many of the clusters investigated contain far more than four water monomers, the percentage water loss for $M_mW_{n>4}H^+$ was not observed to exceed 75%. Thus, methanol loss becomes kinetically competitive before the loss of a fourth water monomer in larger clusters. Given that no evidence was found for direct proton desorption from the cluster (accompanied by just one or two solvent molecules), it can be concluded that cluster structures consisting of a (roughly) central proton with methanol-enriched inner solvation shells are thermodynamically favourable [8,10], and, to a first approximation, the central potential Eq. (1) would seem to be suitable for describing the attractive forces. It should be noted that products arising from water addition (m/z = parent + 18) were not observed on the microsecond quadrupole timescale.

3.2.4. Towards complete proton desolvation under multiple-collision conditions

Even for clusters with a relatively high water content, there was a marked tendency towards dehydration as the number of cluster monomers decreased to fewer than nine. In other words, as the number of monomer units lost due to evaporation increased with collision energy, the fragment ion current became increasingly water-rich, and most, if not all, of the water monomers were lost before the cluster was reduced to fewer than seven methanol molecules. This phenomenon is manifest in the low-mass region of the multiple-collision CID spectra, which were typically dominated by M_mH^+, $m \leq 8$.

An intriguing result of the multiple-collision study was the persistence of low-mass daughter ions of composition $M_xW_3H^+$ ($x \geq 1$) for certain clusters containing three or more water monomers, notably $M_{10,11}W_3H^+$, $M_{12}W_{4–6}H^+$, $M_{11}W_5H^+$, $M_{13}W_6H^+$ (Fig. 7). Typically less intense than the M_mH^+, $m < 7$ daughters, the persistence of these products and the absence of more hydrated CID daughters from which these granddaughters could be derived, is direct evidence for competitive proton solvation in certain clusters containing more than three water monomers. Since a subtitutional interaction (M ↔ W) has been characterised for the extremities of these clusters, and W_4H^+ is a 'magic number' in pure water spectra, some isomers of the above-mentioned $M_mW_{n>3}H^+$ clusters clearly contain an MW_3H^+ core.

4. Conclusions

Charged droplet shrinkage, a key mechanism of ES ion formation, results in a $(solvent)_nH^+$ cluster distribution resembling those generated by EI, FAB and LSIMS, albeit more extensive and without the radical ions observed in FAB/LSIMS experiments. Weak features attributable to structures of high stability are manifest as discontinuities in the log plot of the total number of monomers '$m + n$' versus the abundance sum. Breaks after repeated addition of five to six monomers might be due to the formation of ring structures, however, this deduction is equivocal. For instance, this abundance anomaly could be due to more extensive branching arising from the introduction of water (two donor/one acceptor sites versus methanol with one donor/one acceptor sites). Notwithstanding, information concerning the alignment of the hydrophobic methyl groups, and the role of the methyl hydrogen atoms, polarised by a proximal charge, could not be ascertained. The weight of experimental evidence supports the proton in these clusters occupying a central position, with aggregate growth extending radially from the charge.

Overall, the MS^2 results obtained for the smaller aggregates using the Quattro II are in accordance with those obtained by Karpas et al. [7] and Stace and Shukla [10]. The variation in the nature of the monomer lost (M versus W) with changing cluster composition justifies the selection of low-energy CID for probing the droplet extremities. The dissociation chemistry also suggests methanol-enriched cores are an abundant, although not dominant, structural feature of these mixed clusters. Trace amounts of background water in the CID gas proved to be diagnostically useful regarding the presence of methanol molecules in the water-enriched cluster periphery. To properly exploit this low-energy phenomenon, an accurate knowledge of the water number density in the collision gas is required. The thermoneutral analogue of the M → W substitution, W → W, would be particularly interesting to monitor, as information concerning potentially all of the peripheral monomers could be obtained. This study would require D_2O as a component of the collision gas, and such experiments could prove difficult to implement on a commercial triple quadrupole mass spectrometer. Nevertheless, this study has confirmed the ability of water to substitute methanol in mixed $M_mW_nH^+$ clusters approaching nanoscale dimensions. Proof of competitive proton solvation was also presented, through the persistence of CID daughters with stoichiometry $M_mW_3H^+$ (much less intense than M_mH^+, $m < 7$) which demonstrated a tendency to lose methanol molecules, rather than water, under multiple-collision conditions.

Acknowledgements

The author would like to thank Dr. Jennifer A. Irwin (Plant Industry, CSIRO, Black Mountain, Canberra) for carefully reading and editing this manuscript prior to submission, and Messrs Daniel Gardiner (Geoscience Australia) and Russel Koehne (Electronics Unit, Research School of Chemistry, ANU) for assistance with aspects of the null measurements.

References

[1] Katz, T. Chaudhary, F.H. Field, J. Am. Chem. Soc. 108 (1986) 3897.

[2] J. Sunner, M.G. Ikonomou, P. Kebarle, Int. J. Mass Spectrom Ion Processes 82 (1988) 221.
[3] R.A.W. Johnstone, A.H. Wilby, Int. J. Mass Spectrom. Ion Processes 89 (1989) 249.
[4] Y. Xu, V.M. Jarvis, D.E. Boswick, T.F. Moran, Org. Mass Spectrom. 26 (1991) 892.
[5] M.V. Kosevich, G. Czira, O.A. Boryak, V.S. Shelkovsky, K. Vékey, Rapid Commun. Mass Spectrom. 11 (1987) 1411.
[6] J.E. Szulejko, C.E.C.A. Hop, T.B. McMahon, A.G. Harrison, A.B. Young, J.A. Stone, J. Am. Soc. Mass Spectrom. 3 (1992) 33.
[7] Z. Karpas, G.A. Eiceman, C.S. Harden, R.G. Ewing, J. Am. Soc. Mass Spectrom. 4 (1993) 507.
[8] P. Kebarle, R.N. Haynes, J.G. Collins, J. Am. Chem. Soc. 89 (1967) 5753.
[9] E.P. Grimsrud, P. Kebarle, J. Am. Chem. Soc. 95 (1973) 7939.
[10] A.J. Stace, A.K. Shukla, J. Am. Chem. Soc. 104 (1982) 5314.
[11] M. Meot-Ner, J. Am. Chem. Soc. 108 (1986) 6189.
[12] K. Hiraoka, H. Takimoto, K. Morise, J. Am. Chem. Soc. 108 (1986) 5683.
[13] S. Morgan, A.W. Castleman Jr., J. Am. Chem. Soc. 109 (1987) 2867.
[14] N. Nishi, K. Yamamoto, J. Am. Chem. Soc. 109 (1987) 7353.
[15] S. Morgan, R.G. Keesee, A.W. Castleman Jr., J. Am. Chem. Soc. 111 (1989) 3841.
[16] S. Morgan, A.W. Castleman Jr., J. Phys. Chem. 93 (1989) 4544.
[17] W.J. Herron, M.T. Coolbaugh, G. Vaidyanathan, W.R. Peifer, J.F. Garvey, J. Am. Chem. Soc. 114 (1992) 3684.
[18] M.S. El-Shall, C. Marks, L.W. Sieck, M. Meot-Ner, J. Phys. Chem. 96 (1992) 2045.
[19] A. Wakisaka, H. Abdoul-Carime, Y. Yamamoto, Y. Kiyozumi, J. Chem. Soc. Trans. Faraday Soc. 94 (1998) 369.
[20] G. Raina, G.U. Kulkarni, Chem. Phys. Lett. 337 (2001) 269.
[21] G. Raina, G.U. Kulkarni, C.N.R. Rao, J. Phys. Chem. 105A (2001) 10204.
[22] Y.J. Shi, S. Consta, A.K. Das, B. Mallik, D. Lacey, R.H. Lipson, J. Chem. Phys. 116 (2002) 6990.
[23] W.Y. Feng, C. Lifschitz, Int. J. Mass Spectrom. Ion. Processes 149/150 (1995) 13.
[24] R.G. Ewing, G.A. Eiceman, J.A. Stone, Int. J. Mass Spectrom. 193 (1999) 57.
[25] W. Christen, U. Even, Eur. Phys. J. 16D (2001) 87.
[26] M. Meot-Ner, J. Am. Chem. Soc. 114 (1992) 3312.
[27] X. Yang, A.W. Castleman Jr., J. Am. Chem. Soc. 111 (1989) 6845.
[28] A.J. Stace, C. Moore, J. Am. Chem. Soc. 105 (1983) 1814.
[29] C. Chaudhuri, J.C. Jiang, X. Wang, Y.T. Lee, H.-C. Chang, J. Chem. Phys. 112 (2000) 7279.
[30] P. Kebarle, Y. Ho: On the mechanism of electrospray mass spectrometry, in: R.B. Cole (Ed.), Electrospray Ionisation Mass Spectrometry: Fundamentals, Instrumentation and Applications, Wiley, New York, 1997 (Chapter 1).
[31] P.H. Dawson, J.B. French, J.A. Buckley, D.J. Douglas, D. Simmons, Org. Mass Spectrom. 17 (1982) 205.
[32] Micromass UK Ltd., Floats Rd, Wythenshawe, Manchester M23 9LZ, UK.
[33] R.A. Provencal, J.B. Paul, K. Roth, C. Chapo, R.N. Casaes, G.S. Tschumper, H.F. Schaefer III, R.J. Saykally, J. Chem. Phys. 110 (1999) 4258.
[34] T. Su, M.T. Bowers, Classical Ion–Molecule Collision Theory, in: M.T. Bowers (Ed.), Gas Phase Ion Chemistry, vol. 1, Academic Press, New York, 1979, p. 83 (Chapter 3).
[35] J. Hine, K. Arata, Bull. Chem. Soc. Jpn. 49 (1976) 3089.
[36] E.P. Hunter, S.G. Lias, J. Phys. Chem. Ref. Data 27 (1998) 413.
[37] D.R. Lide (Ed.), CRC Handbook of Chemistry and Physics, 73rd ed., CRC Press, Boca Raton, FL, 1993.